Theoretical study of disorder in Ti-substituted La$_2$Zr$_2$O$_7$

Alain Chartier and Constantin Meis*

CEA-Saclay DEN/DPC/SCPA Bâtiment 450, 91191 Gif-Sur-Yvette, France

William J. Weber and L. René Corrales[†]

Pacific Northwest National Laboratory, P.O. Box 999, Richland, Washington 99352

Pyrochlores have the striking feature that their radiation resistance is highly dependent on their composition. In this work, the propensity of a pyrochlore to transform to a cation-disordered structure and the influence of titanium ions is ascertained from the mechanisms of defect formation. A detailed study of defect formation and migration activation energies in Ti-substituted La$_2$Zr$_2$O$_7$ is carried out by modern theoretical computational methods that include the use of a classical interatomic potential with a modified shell model to capture the effects of local charge transfer. The results show that La$_2$Zr$_2$O$_7$ has a tendency towards cation disorder, whereas, substitution of Zr with Ti makes this tendency energetically less favorable.

I. INTRODUCTION

Pyrochlore oxide materials have unique properties, such as the ease with which actinide ions are incorporated,[1] that make them ideal candidates for use in the immobilization of nuclear waste. In addition, pyrochlores and their mineral analogs are quite durable, with leaching rates as low as 10^{-5} g m^{-2}/day at pH$=7$.[2–4] One striking property that distinguishes pyrochlores from one another is that their radiation resistence is highly dependent on composition. For example, titanate pyrochlore compounds that have been proposed for radionuclide immobilization[5,6] readily undergo amorphization under irradiation.[7–9] In contrast, recent experimental results[10–13] have shown that zirconate pyrochlores are highly radiation resistant, remaining crystalline at high doses for time periods equivalent to a million years or more. Amorphization can lead to an increase in volume and compromise the chemical durablility, whereas the crystalline fluorite structure can be more radiation resistant than the initial pyrochlore. The propensity of ions to create Frenkel defects and cation disorders is believed to form the basis with which to ascertain the stability of pyrochlores[10,13] and, thereby, dictate the state to which they might transform. A set of experiments can be carried out, where systematic substitutions of the cations in the lattice are made, to better understand the composition dependence of structural transformations. An extensive study[10,14] on Gd$_2$Zr$_{2(1-y)}$Ti$_{2y}$O$_7$ with $0 \leqslant y \leqslant 1$ demonstrated that radiation resistance decreases with increasing Ti and that Ti-rich compositions ($y \geqslant 0.5$) readily undergo radiation-induced amorphization at low doses even at relatively high temperatures. This supports the observation that under irradiation several zirconate pyrochlores undergo transition to a cation-disordered fluorite structure,[10] which is argued to be the final radiation-damage state for Zr-rich pyrochlores, regardless of the starting structure.[10,13]

A similar systematic approach can also be used for an atomic-level theoretical study. Ideally, it would be useful to study the same systems, i.e., Gd$_2$Zr$_2$O$_7$, as those studied experimentally, however, it is necessary to start with systems that are accessible using currently available theoretical tools.

A readily approachable system by both *ab initio* and classical potential methods is that of La$_2$Zr$_2$O$_7$. At first it would appear that a systematic study of defect formation in La$_2$Zr$_{2(1-y)}$Ti$_{2y}$O$_7$ with a systematic increase of Ti is not feasible because pure lanthanide titanate exists as a layered perovskite, not a pyrochlore. This is resolved by the fact that the pyrochlore structure of lanthanide zirconate exists for a range of stoichiometric composition[15] up to over 1500°C.[16] Therefore, for low concentrations of Ti-substituted La$_2$Zr$_2$O$_7$ the pyrochlore structure is expected to be preserved and so the tendency towards cation disorder can be explored. In this work, modern theoretical computational methods are used to investigate the changes that occur in the formation and migration of defects as Ti is substituted for Zr in La$_2$Zr$_2$O$_7$.

Pyrochlore oxides have the general formula $A_2B_2O_7$, where A and B are metallic cations that can be either trivalent and tetravalent or divalent and pentavalent, respectively. Only the former pair is considered here. In ordered pyrochlores, there is a site in the oxygen sublattice that is systematically vacant; whereas, the fluorite structure has partial occupancy of that particular oxygen site along with disorder of the cations. Cation disorder occurs by the exchange of A and B metal ion sites to form cation antisites. The cation and anion lattice-migration activation energies towards adjacent vacancies in the pyrochlore structure together with the cation antisite and Frenkel-pair formation energies can provide valuable information on the final radiation-damage state of zirconate pyrochlore.[13,17] Changes in cation disorder and oxygen-migration properties, as Ti is substituted for Zr in La$_2$Zr$_2$O$_7$, can be related to the propensity of structural phase changes and is expected to provide an insight on the reasons why the titanate-rich pyrochlores do not undergo a transition towards the disordered fluorite structure.

La$_2$Zr$_2$O$_7$ can be synthesized in many ways (see, for example, Ref. 16 and references therein), including hydrothermal synthesis[18] and sol-gel routes.[19] For slight understoichiometric changes in La$_2$O$_3$ or ZrO$_2$, the cell volume decreases or increases, respectively.[20] For high stoichiometric deviations, there is a phase separation into disordered fluorite and pyrochlore structures.[15] The La$_2$Zr$_2$O$_7$ pyrochlore structure

65 134116-1

TABLE I. Comparison between experimental (Refs. 21,25–29) and calculated data for pure $La_2Zr_2O_7$. HF is for *ab initio* Hartree-Fock calculations with CRYSTAL98, (Ref. 30) AIP is for analytic-Interatomic-Potential calculations done with GULP (Ref. 31) using the parameters (see Table IV) for Buckingham potentials fitted on experimental and HF data. The comparison between experimental and AIP-calculated entropy-versus-temperature curves is shown in Fig. 3.

$La_2Zr_2O_7$	Expt.	HF	AIP
$V(\text{Å}^3)$	315.4	331.5	315.4
a (Å)	10.805	10.986	10.805
x	0.4200	0.4198	0.4202
B (GPa)		191	192
$B'(\text{GPa/Å}^3)$		3.62	
C_{11} (GPa)		335	336
C_{12} (GPa)		120	120
C_{44} (GPa)			101
$S_{300\,K}$(J/mol K)	239.9		235.5
α (10^{-6} K^{-1})	7.0/9.1		6.96

has the space group $Fd\bar{3}m$ that derives from the MO_2 fluorite-like arrangement of atoms.[21,22] The cubic pyrochlore has been widely presented in many publications (see, for example, Refs 17, 23, and 24) and is only briefly described here. The cubic-pyrochlore structure can be described by two independent parameters: the internal parameter x, for the O_{48f} positions, and the cell parameter a. The La^{+3} ions occupy the special site 16d (1/2,1/2,1/2) (A site) and the Zr^{+4} ions occupy the special site 16c (0,0,0) (B site).[21] The oxygen atoms are located at sites 48f (x,1/8,1/8) (denoted O_{48f}) and 8b (3/8,3/8,3/8) (denoted O_{8b}), which are independent because of their local environment. The site of the missing oxygen that could complete the anion sublattice to form a fluorite structure is 8a (1/8,1/8,1/8) (denoted O_{8a}). Interstitial atoms may be accomodated into the 32e site (1/4,1/4,1/4). The experimental parameters are reported in Table I and a d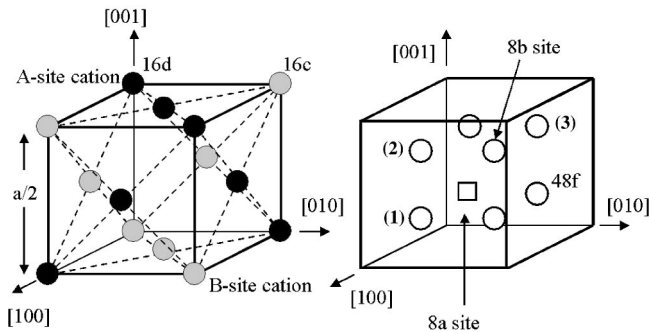rawing of the structure is shown in Fig. 1. (Note that alternative crystallographic definitions are possible and exist in the literature.) The O anions are differentiated because of differences in the local molecular environment as follows. O_{8b} is surrounded by four A^{+3} cations, $V_{O_{8a}}$ (the O vacancy) is surrounded by four B^{+4}, and O_{48f} is surrounded by two A^{+3} and two B^{+4} cations where all the cations are in a tetrahedral configuration with respect to the O (or vacancy) center. Thus, in the ordered pyrochlore, a difference in the electronic structures of the O_{48f} and O_{8b} oxygens should be expected. In contrast, this should not be the case in the disordered fluorite structure, since the cations are expected to be randomly distributed between the A and B sites, while oxygens may partially occupy the 8a sites as well as the other anion sublattice sites. In the fluorite configuration, a homogeneous electronic structure should be expected for the oxygen anions.

It is of upmost importance that the force field destined for the study of defects in $La_2Zr_{2(1-y)}Ti_{2y}O_7$ be capable of reproducing the crystallographic positions and the experimentally known physical properties up to a satisfactory degree. In fact, a correct reproduction of the elastic properties, the vibration entropy, the infrared and Raman spectra, and of the thermal expansion requires that the ionic interactions be well described by the interatomic potentials not only at the equilibrium positions but also at intermediate distances.[32] Lanthanum zirconate pyrochlore has the advantage that its physical properties, such as crystallographic parameters,[33,21,25,26] Raman and infrared spectra,[33] vibrational entropy,[27] thermal-expansion coefficient,[28,29] and phase diagram,[15] have been extensively studied making it an excellent benchmark system. Consequently, the theoretical models can be compared with a robust experimental database before applying them to study defects.

The computational study is carried out using the *ab initio* codes CRYSTAL98 (Ref. 30) and CASTEP.[34] The results from the Hartree-Fock (HF) *ab initio* calculations are used to develop an analytic interatomic potential (AIP), which includes a modified shell-model component to capture the effects of charge transfer. The Ti-O potential is established in the specific geometric configuration of the $La_2Zr_2O_7$ structure, using the same ionic charges and polarizability, so that transferability conditions are met. Thus, both the $La_2Zr_2O_7$ and $La_2Ti_2O_7$ systems in the pyrochlore cubic structures are optimized using the HF *ab initio* method. The HF results for $La_2Ti_2O_7$ in the corresponding cubic symmetry, which does not exist in nature, are used to establish a reliable and transferable interaction potential for the Ti-O interaction. An accurate AIP is useful to carry out the more complex calculations of cation disorder and ion migration that remain computationally prohibitive for *ab initio* calculations. The classical calculations are carried out using the GULP code.[31]

This paper is organized as follows. In Sec. II, the details of our computational approach are provided. The optimized structures obtained from *ab initio* and interatomic approaches are described in Sec. III. Detailed results and discussions of the defect formation energies are given in Sec. IV and those for the activation energies are given in Sec. V. Finally, conclusions are given in Sec. VI.

FIG. 1. The $La_2Zr_2O_7$ pyrochlore structure separated into cation and anion sublattices. Zirconium occupies the 16c site and lanthanum the 16d site. The vacancy (at 8a) is tetrahedrally coordinated by four zirconium (16c) cations and O_{8b} is tetrahedrally coordinated by four lanthanum (16d) cations. The labels (1), (2), and (3) on the anion sublattice correspond to the oxygen-lattice migration referred to in Table IX.

II. COMPUTATIONAL DETAILS

The implementation of the *ab initio* self-consistent field (SCF) HF linear-combination-of-atomic-orbitals (LCAO) computational scheme within the CRYSTAL98 code (Ref. 30 and references therein) is well described in the literature (see, for example, Refs. 35 and 36). The basis sets in this work for lanthanum, zirconium, titanium, and oxygen are all-electron Gaussian-type orbitals (see Ref. 37). The f orbitals are not included in the lanthanum basis that CRYSTAL98 uses, however, to first order they are not expected to make a major contribution to the structural features of this system. The external *sp* exponents of the valence part of the basis set have been optimized using the experimental pyrochlore geometry. The controls for the direct space summations of the Coulomb and exchange series are set to values of 7, 7, 7, 8, and 15 corresponding to high numerical accuracy. The shrinking factor was set to 4 corresponding to a regular mesh of eight **k** points in the reciprocal space. The calculations were carried out using unrestricted Hartree-Fock (UHF) theory that allows the electrons to be unpaired. The calculated energies for the cation-antisite defects were corrected *a posteriori* for the exchange and correlation term by using a correlation-only functional established by Perdew and co-workers (quoted PD91).[38,39] This is necessary because HF theory does not contain correlation.

In parallel to the *ab initio* CRYSTAL98 code, an AIP evaluated within the GULP code[31] was used. Based on experimental data and on the HF-calculated elastic properties, a force field was established for the description of $La_2Zr_2O_7$ pyrochlore. The interatomic potential is composed of short-ranged two-body ionic interactions of the Buckingham type that complement the Coulomb interactions. As is well known, Buckingham potentials are composed of a Born-Mayer repulsive exponential term and an r^{-6} attractive term. The Buckingham-type cation-cation interactions are set to zero while maintaining the electrostatic interactions. The ionic polarizability is taken into account by using a modified classical shell model of Dick and Overhauser[40] that consists of a shell that can shift about the central core to mimic shifts in the electron cloud. A harmonic spring constant characterizes the interaction between the core and the shell of a given ion. The modification in this work consists of adapting the Mulliken analysis of the UHF-optimized structures for the fractional charge of the core.

Cation-antisite-disorder energies were calculated, within the AIP, the UHF+PD91, and also by a density-functional-theory[41] (DFT) approach, using the CASTEP package.[34] The latter was applied using a plane-wave ultrasoft pseudopotential basis[34] within the local-density approximation[41] (LDA) and Pulay's charge-density-mixing scheme with an amplitude of $Q_{max}=0.8$ and a cutoff of 1.5. The SCF convergence criterion was fixed to 10^{-5} eV/atom.

The *ab initio* calculations of the different cation-disorder configurations were carried out using the primitive unit cell with periodic boundary conditions (PBC). Within the AIP model, both PBC and the Mott-Littleton approximation (MLA) were used.[42] In the MLA method, the crystal bulk is divided into two concentric spherical regions centered on the
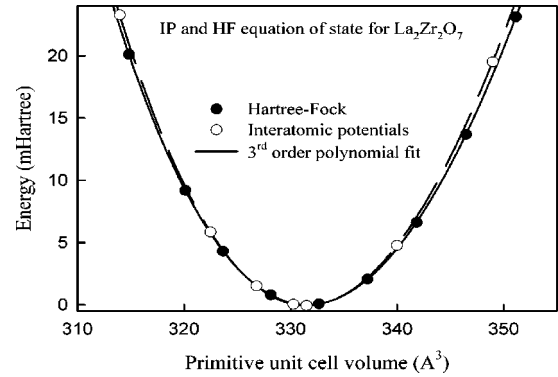

FIG. 2. Energy (mHartree) versus primitive-unit-cell-volume ($Å^3$) curves for $La_2Zr_2O_7$ using AIP and HF methods. Optimized volumes of the AIP calculation have been shifted to HF optimized volumes and minimum energy has been shifted to zero for comparison.

defect. In the first one, the interactions are treated rigorously and the ions are allowed to fully relax. In the second region, only harmonic perturbations are considered. There is also an outer region surrounding the two concentric regions where the ions interact with the defect net charge as in a perfect dielectric medium. The activation energies for the ion-lattice migration were calculated by using transition-state theory where the saddle-point search was carried out using the rational-function-optimization (RFO) algorithm,[43] as implemented in the GULP code.

III. STRUCTURE VALIDATION

A. *Ab initio* HF calculations

The internal structural parameter x was optimized at constant volume for the two cubic compounds $La_2Zr_2O_7$ and $La_2Ti_2O_7$ using nine different values of the volume for each structure. The initial volume considered for $La_2Ti_2O_7$ is that of the layered-perovskite,[44] which is very close to that of a hypothetical cubic pyrochlore.[13] The energy-versus-volume results were fit using the Birch-Murnaghan equation of state[45,46] shown in Fig. 2. The optimized volumes, the bulk modulus B, and its first derivative B' with respect to the volume were determined. The two elastic constants C_{11} and C_{12} were calculated by carrying out deformations of the cubic structure (strain matrix as in Ref. 30 or Ref. 47) independent of the analytical relation between the bulk modulus and these constants. The results are presented in Tables I and II. As expected, the calculated volumes overestimate, by about 5%, the experimental ones.[35,48] However, the calculated internal parameter x for $La_2Zr_2O_7$ is in good agreement with the experimental value. To our knowledge, no experimental data are available for the bulk modulus, its first derivative with respect to volume, and the elastic constants, for comparing to the calculated values. It should be noted that, for both $La_2Zr_2O_7$ and $La_2Ti_2O_7$, the bulk modulus B obtained with the calculated elastic matrix constants by the relationship $B=(C_{11}+2C_{12})/3$, is close to that deduced by the Birch-Murnaghan equation of state. Finally, the first derivatives of the bulk modulus with respect to the volume, B', are

TABLE II. Comparison between HF and AIP calculated data for pure $La_2Ti_2O_7$. Symbols are defined in Table I. Experimental volume is $278.5 Å^3$ for layered perovskite $La_2Ti_2O_7$ (Ref. 44) and it is equivalent to $a = 10.366 Å$, considering a cubic cell.

$La_2Ti_2O_7$	HF	AIP
$V(Å^3)$	292.8	278.5
$a(Å)$	10.541	10.366
x	0.4272	0.4267
B (GPa)	221	222
$B'(GPa/Å^3)$	3.83	
C_{11} (GPa)	379	376
C_{12} (GPa)	144	144

TABLE IV. Interatomic parameters for Buckingham potentials fitted on experimental and HF-calculated physical values quoted in Table I. Charges satisfy $Q^{core} + Q^{shell} = Q^{formal}$ and $Q^{core}_{O48f} = -1.65, Q^{core}_{O8b} = -1.90, Q^{core}_{La} = +2.90, Q^{core}_{Zr} = +3.20$, and $Q^{core}_{Ti} = +2.90|e|$, see text.

Ions	A(eV)	ρ(Å)	C(eV Å^6)	$\mathbf{k}$(eVÅ^{-2})
O-O	22764.3	0.14900	27.89	O_{8b} : 261.8
				O_{48f} : 280.2
La-O	1183.8	0.36565	0.00	221.5
Zr-O	1872.5	0.34138	0.00	235.0
Ti-O	1256.2	0.34927	0.00	236.0

very close to the expected value of 4, generally found for the majority of similar compounds[46] demonstrating the very satisfactory coherence characterizing the HF results.

The electronic charge of the ions in both pyrochlores was calculated using the Mulliken-analysis approach as implemented in the electronic-structure codes. The results are listed in Table III for the ordered (0X) $La_2Zr_2O_7$ and $La_2Ti_2O_7$. The total charge on the lanthanum ion is roughly $+2.9|e|$ in both pyrochlores, thus very close to the formal charge, while that on zirconium is between $3.23|e|$ and $3.25|e|$, identical to that calculated for zirconia (ZrO_2).[49] The calculated titanium charge is $+2.90|e|$, about 3% higher compared to that calculated in rutile TiO_2.[50] As anticipated from the differences in the local molecular environment, two different net charges were obtained for the oxygens. The O_{8b}, lying in the center of a lanthanum-ion tetrahedra, carries a net charge of roughly $-1.90|e|$, close to the formal value of $-2.0|e|$. Whereas, O_{48f}, in the center of a tetrahe-

dron made up of two La and two Zr cations, has a net charge of $-1.73|e|$ and $-1.61|e|$ in $La_2Zr_2O_7$ and $La_2Ti_2O_7$, respectively.

B. Analytic-interatomic-potential-based calculations

The AIP consists of the Coulomb interactions for the ionic interactions, the Buckingham potential for the packing forces, and the modified shell model that captures short-range charge-transfer and polarization effects. The GULP fitting procedure[31] was used to optimize the parameters of the AIP for both pyrochlores. The fitting for $La_2Zr_2O_7$ was based on the experimental values of the lattice parameter, the atomic positions, and the vibration entropy at 300 K. In addition, the HF-calculated bulk modulus and elastic matrix constants were used, even though they are usually overestimated by about 5–10 % within this approach.[48,51] The parameters for $La_2Ti_2O_7$ used the crystallographic data and elastic properties obtained from the HF calculations. The Mulliken charges determined by the electronic- structure code were used in parametrizing the shell model for both the cations and the anions. For the latter, two different oxygen sites, 48f and 8b, were modeled. This is in accord with previous studies that revealed the importance of distinguishing the oxygens in the pyrochlore structure, resulting in a very successful representation.[17,24] The total charge (shell +core) on each ion was set equal to its formal charge permitting a direct substitution of titanium for zirconium, where the core charge was set equal to the partial charge obtained from the Mulliken charge analysis of the UHF-optimized structure. The parameters determined in this work are shown in Table IV. The parameters of the O-O Buckingham potential were set equal to previously published values.[52] In Tables I and II, the optimized results for the AIP model are given. The results are quite satisfactory for all the observables included in the fitting procedure. Indeed, the agreement between the HF and AIP model on the energy-versus-volume variation for $La_2Zr_2O_7$ in Fig. 2 shows the quality of the force-field optimization using the HF-calculated elastic properties. Also, the calculated entropy at 300 K of 235.5 J mol^{-1} K^{-1} is very close to the experimental value[27] of 239.9 J mol^{-1} K^{-1} used in the fitting procedure, while the temperature dependence within the range 0–1000 K, represented in Fig. 3, is in excellent agreement with experiment.

TABLE III. Mulliken charges (in terms of $|e|$) calculated using the HF method. 0X, 1X, and 2X denote, respectively, no disorder, one La^{3+}-Zr^{4+} inversion, and two La^{3+}-Zr^{4+} inversions.

$La_2Zr_2O_7$	Site A	Site B	Oxygen	
			O_{48f}	O_{8b}
0X [a]	La= +2.907	Zr= +3.250	−1.733	−1.916
0X [b]	La= +2.905	Zr= +3.229	−1.726	−1.912
1X [b]	La= +2.876	Zr= +3.196	−1.663	−1.841
	La= +2.906	Zr= +3.274	−1.725	−1.846
	Zr= +3.275	La= +2.876	−1.841	
2X [b]	La= +2.874	Zr= +3.178	−1.741	−1.752
	La= +2.893	Zr= +3.305	−1.758	−1.802
	Zr= +3.302	La= +2.822	−1.805	
	Zr= +3.321	La= +2.875		
$La_2Ti_2O_7$				
0X [a]	La= +2.898	Ti= +2.907	−1.616	−1.916

[a]Calculation done with fully optimized geometry using HF method (Table I).

[b]Single-point energies on the optimized geometry obtained using AIP method.
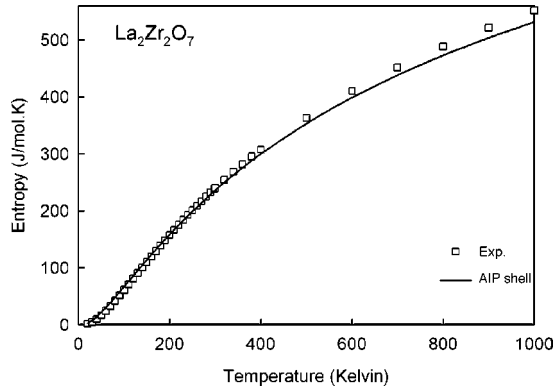
FIG. 3. Entropy ($J\,mol^{-1}\,K^{-1}$) versus temperature (kelvin) for pure $La_2Zr_2O_7$. Shown is the curve (solid line) calculated using the AIP shell model and is compared to experimental data (circles).

The entropy, obtained from the phonon spectra, was calculated over a grid covering 10-K symmetry-unique points across the Brillouin zone.

Further validation of the current potentials is obtained from the calculated thermal-expansion coefficient α as determined from the shell-model molecular-dynamics simulations. The value thus obtained, given in Table I, is equally in good agreement with the experiment.[28] Finally, the calculated infrared lattice-vibrational frequencies as well as the Raman frequencies, presented in Table V, are well correlated with the experimental values.[33]

The current AIP model is quite satisfactory on the whole and the ionic interactions appear to be reproduced reliably by the corresponding short-range analytical potentials. Consequently, it can be applied with confidence to study defect formation and migration energies in $La_2Zr_{2(1-y)}Ti_{2y}O_7$.

IV. DEFECT FORMATION ENERGIES

A. Cation-antisite disorder in pure and Ti-substituted $La_2Zr_2O_7$

Under continuous irradiation, a large number of cation antisites can accumulate in a localized volume of the bulk. In such a disordered configuration, the interactions among the defects of the neighboring lattice sites, a purely collective phenomenon, strongly affect the cation-antisite formation energy and should differ from that of an isolated antisite defect in a perfect pyrochlore bulk. It is intriguing that the method

TABLE V. Comparison between experimental and AIP- (using Buckingham-potential parameters quoted in Table IV) calculated vibrational properties for pure $La_2Zr_2O_7$. Infrared vibrational frequencies have been assigned by their values.

$La_2Zr_2O_7$ (cm^{-1})	Infrared lattice-vibrational energies						
	ν_1	ν_2	ν_3	ν_4	ν_5	ν_6	ν_7
Exp. (Ref. 33)	518	412	352	244 / 208	176	140	101
AIP	453	391	349	238 / 186	158	119	99
	Energies for Raman frequencies (cm^{-1})						
Exp. (Ref. 33)	743	590	523	498	395	298	
AIP	690	600			387	290	

of calculation, that is, the MLA or the PBC, can yield the behavior at two extreme points of irradiation. The MLA, generally used for the calculations of point defects embedded in an infinite ideal crystal, can give information on the anti-site formation energies that are associated with isolated disorder. Whereas, using supercells, containing at least one cation antisite per primitive unit cell, should be more appropriate for the estimation of the radiation-induced antisite formation energies related to the accumulation of defects that are associated with a longer-range interaction. Thus, the MLA can be used to characterize behavior in the ordered pyrochlore at the onset of irradiation, whereas, the PBC can be used to characterize the response under irradiation of an ordered pyrochlore at the end stage. In the case of accumulating defects, the number of possible configurations to simulate is extremely large, prohibiting an exhaustive computational study. Thus, as a first approximation, the simpler way to proceed is to consider a single cation-antisite defect per primitive unit lattice and apply PBC conditions for the energy optimization. Certainly, such a homogeneous antisite distribution in the bulk is less physical than a statistical one, nonetheless there is an interesting and useful comparison with the corresponding MLA calculations. For these reasons, both MLA and PBC computational approaches were used. The defect energies were calculated using the classical scheme of $E_{defect} = E$ (relaxed bulk with defect) $- E$ (relaxed perfect bulk) $+ \Delta E_\infty$, where ΔE_∞ is the energy correction corresponding to the interaction among the various sublattices at infinite distance. For the AIP used here, ΔE_∞ vanishes because the analytical potentials are defined to be zero at infinite distance. This is generally not the case in first-principles calculations for charged vacancies, where the missing ion is assumed to be at an infinite distance from the crystal, requiring a delicate operation for the estimation of the ΔE_∞ quantity. Therefore, since *ab initio* isolated point-defect calculations are very expensive within the MLA, only AIP modeling was used. The first principles calculations were applied only to disordered configurations without vacancies, in which cases $\Delta E_\infty = 0$. Whereas, three different computational methods, AIP, HF and DFT/LDA, were employed for the periodic lattice system based on the primitive unit cell of $La_2Zr_2O_7$ containing 22 atoms. In this way, a straightforward comparison can be made between the periodic-system AIP results and those obtained from the single-point-energy first-principles calculations, carried out exactly on the same configurations of the AIP fully relaxed periodic system.

The disorder was simulated by the crystallographic site exchange of La and Zr ions, around the O_{48f} oxygen. A single La-Zr exchange is denoted by $1X$ while a double one, corresponding to a higher degree of disorder, by $2X$ (see Table III). The influence of titanium on the structure was also studied by two different means. In the first, a titanium ion was substituted for zirconium close to an isolated cation-antisite defect within the Mott-Littleton approach. In the second, supercells of $La_2Zr_{2(1-y)}Ti_{2y}O_7$ were considered with low titanium concentrations ($y \leq 0.5$) to avoid any structural transition to the perovskite phase. Again, a large number of possible configurations may result in the last case, but only a couple of typical situations were considered here. A single

TABLE VI. Cation-antisite-disorder energies (eV) for the compact configuration around the $48f$ site, calculated using Mott-Littleton approach and periodic primitive cell with analytic-interatomic-potentials method (AIP), *ab initio* Hartree-Fock with *a posteriori* correction of correlation established by Perdew and co-workers (Refs. 38 and 39) (UHF+PD91) and DFT LDA (DFT) (Ref. 34) n(Ti) indicates the number of Ti-atoms considered in Mott-Littleton calculations.

| Disorder | Ti-substituted $La_2Zr_2O_7$ Mott-Littleton approach | | $La_2Zr_{2(1-y)}Ti_{2y}O_7$ Periodic primitive cell | | | |
	n(Ti)	AIP	y	AIP	UHF+PD91	DFT
$0X$	0	0.00	0.00	0.00	0.00	0.00
$1X$	0	1.95	0.00	1.45	2.49	1.96 (1.38)
$2X$	0	3.37	0.00	2.79	6.88	5.28 (2.60)
$0X$	1	0.00	0.25	0.00	0.00	0.00
$1X$	1	1.53	0.25	1.08	2.28	1.61
$1X$-1Ti	1	3.62	0.25	1.60	3.45	2.41
$2X$	1	3.00	0.25	1.59	3.41	2.42
$0X$	2	0.00	0.50	0.00	0.00	0.00
$1X$	2	1.72	0.50	0.70	1.88	1.40
$1X$-1Ti	2	4.08	0.50	1.23	2.85	2.00
$2X$	2	4.09	0.50	1.21	2.84	2.04

substitution of Ti for Zr is denoted by 1Ti and a double one by 2Ti. A single La-Ti crystallographic site exchange is denoted by $1X$-1Ti (see Table VI).

The Mott-Littleton calculated energy for $1X$ in pure (y=0) $La_2Zr_2O_7$ is 1.95 eV, considerably lower than the values of 4.4–4.8 eV determined by Minervini et *al*.[53,13] At this point, it is worth noting that significant discrepancies result from the AIP calculations of defect energies in similar cases. For example, Williford et *al*[17] calculated the 1X (Gd-Ti) antisite formation energy in $Gd_2Ti_2O_7$ pyrochlore to be 3.53 eV, also considerably lower, roughly by a factor of two, compared to the 5.6–6.0 eV published by Minervini and co-workers,[53,13] while Catlow obtained the value of 1.5 eV.[52] It is likely that the different force fields used for each of the calculations are the origin of these discrepancies. Although it is just as likely that differences are due to the local asymmetric structure of the crystal, such as the distinct environment of the $48f$ and $8b$ oxygen sites as well as that there are two A-B cation nearest neighbor-distances that are not accounted for by those potentials. Also, there are distinct differences in using the MLA and PBC, as discussed above. To further check the validity of the AIP results obtained here, single-point-energy *ab initio* calculations with PBC on the AIP-optimized periodic geometries were carried out using the UHF+PD91 (CRYSTAL98) and DFT/LDA plane-wave (CASTEP) methods. The results, also given in Table VI, are in satisfactory agreement with the AIP calculations. Due to the high computational cost, it was out of the question to carry out full constant-pressure relaxations within the HF and the DFT/LDA for all the antisite configurations quoted in Table VI. Nevertheless, for validating the consistency of the single-point-energy calculations on the AIP-optimized geometries, a full relaxation study for the $1X$ and $2X$ configurations in $La_2Zr_2O_7$ was performed using the DFT/LDA (CASTEP) resulting in the values of 1.38 eV and 2.60 eV, respectively (in

parenthesis Table VI). These values are close to the AIP-calculated ones with PBC. Consequently, in pure (y=0)$La_2Zr_2O_7$ a comparison of the MLA values with those of the PBC AIP shows that the cation-antisite inversion occurs more easily in a disordered structure than in the ordered pyrochlore. This could be interpreted as different behavior under irradiation between an ordered pyrochlore and a disordered state, where in the latter the disorder particularly favors the cation exchange at a very low energy cost.

Following the values presented in Table VI, it appears that the influence of titanium ions is contradictory between the MLA and the PBC approach. In fact, for increasing titanium concentration, the cation-antisite formation energies, $1X$-1Ti and $2X$, increase in the MLA approach, while they decrease in the PBC approach no matter what method is used (AIP, HF, or DFT/LDA). This could mean that the effect of cation disorder is far more preponderant than the titanium influence. It is very important to note that in all cases quoted in Table VI, the $1X$-1Ti antisite energy corresponding to a La-Ti exchange is higher than the corresponding La-Zr exchange by $\sim$140% in the MLA case and by $\sim$50% in the PBC case. The strong inhomogeneous behavior among the cation exchange possibly leads to a weak lattice stability of the ordered Ti-doped pyrochlore under irradiation. This effect is less pronounced in the Ti-doped disordered state, even though in this case the lattice instability is large. Despite the lower absolute values obtained here for the cation-antisite formation energies as compared to those previously published, the relative energy difference between $1X$ (La-Zr) and $1X$-1Ti (La-Ti) has the same trend as that estimated by Minervini and co-workers[53,13] That work shows an increase of about 26% for the antisite energies from the pure end-member zirconate up to the pure end-member titanate.

A high degree of antisite accumulation leads to the transition from the pyrochlore to the disordered-fluorite structure

TABLE VII. Defect formation energies for oxygens (eV/defect) in different antisite-disorder configurations, using Kroger-Vink notation.

$La_2Zr_2O_7$ defects	Pure			Ti substituted for Zr	
	$2X$	$1X$	$0X$	$0X$-1Ti	$0X$-2Ti
O_{8a}^{2-} (shell model of O_{48f}^{2-})	-14.96	-15.53	-15.64	-14.77	-13.97
O_{8a}^{2-} (shell model of O_{8b}^{2-})	-14.96	-15.55	-15.64	-14.77	-13.97
$V_{O_{48f}}^{\cdot\cdot}$	16.80	15.86	18.70	17.86	17.09
$V_{O_{48b}}^{\cdot\cdot}$	16.75	15.75	19.54	19.41	19.72
O_{8a}^{2-}-$V_{O_{48f}}^{\cdot\cdot}$ (extended)	1.84	0.33	3.06	3.09	3.12
O_{8a}^{2-}-$V_{O_{48b}}^{\cdot\cdot}$ (extended)	1.79	0.22	3.90	4.64	5.75
O_{8a}^{2-}-$V_{O_{48f}}^{\cdot\cdot}$ (close)	-1.64	-0.15	-0.05	0.20	0.13
O_{8a}^{2-}-$V_{O_{48b}}^{\cdot\cdot}$ (close)	-2.87	-0.20	1.28	0.17	0.20

and the cation environment switches from scalenohedron[54] to octahedra. The Mulliken charge analysis on the single-point-energy calculations with the AIP-optimized geometry (quoted in Table III) reveals the La and Zr charges to suffer negligible variations by the antisite disorder ($1X$ or $2X$). This is not the case for the oxygen charges that, as expected, are strongly affected by the antisite configurations converging smoothly to a unique value: $-1.84|e|$ for $1X$ and $-1.80|e|$ for $2X$. This oxygen-charge homogenization with increasing cation disorder is an indication that the disordered pyrochlore structure gets closer to a fluorite-like one. This will be further correlated to the cation and anion Frenkel-pair formation energy as well as to the activation energies for lattice migration in the following sections.

B. Cation and anion defects

The vacancy and interstitial formation energies for all the cations and anions were calculated using the AIP within the MLA. The aim was to estimate the disorder and the titanium influence. The calculations were performed in pure $La_2Zr_2O_7$ at $0X$, $1X$, and $2X$ disorder, as well as in the neighbor of one ($0X$-1Ti) or two ($0X$-2Ti) titanium ions substituted for zirconium in the ordered pyrochlore.

The lattice stability when incorporating a supplementary oxygen in the pyrochlore-vacant site $8a$ was examined first. Using the charges and polarizabilities of either O_{48f}^{2-} or O_{8b}^{2-} for the oxygen O_{8a}^{2-} leads to identical results as shown in Table VII. The negative values obtained demonstrate the strong tendency of the system to become overstoichiometric $La_2Zr_2O_{7+z}$, which is not significantly influenced by increasing disorder or titanium substitution. Furthermore, insertion of a supplementary oxygen in the $32e$ site leads to the occupancy of the $8a$ site after full relaxation. Again, there is no change in this tendency with the degree of disorder or titanium concentration, nor does it depend on the oxygen shell model used (O_{48f}^{2-} or O_{8b}^{2-}). This behavior is in agreement with the experimental observations carried out on $Ce_2Zr_2O_7$ (Ref. 55) where oxygen insertion was observed to have a very strong preference for the $8a$ site rather than the $32e$ one.

Titanium produces a negligible effect on oxygen vacancy formation. Conversely, the disorder has a net influence on

both $V_{O_{48f}}^{\cdot\cdot}$ and $V_{O_{8b}}^{\cdot\cdot}$ by diminishing the corresponding formation energies (Table VII). The calculated close Frenkel-pair, $O_{8a}^{2-} + V_{O_{48f}}^{\cdot\cdot}$, formation energy is -0.05 eV, in good correlation with the zero value found experimentally in $Gd_2(GaSb)_{0.2}Zr_{1.6}O_7$.[56] The close Frenkel-pair formation energy decreases with increasing disorder (Table VII) entailing a quasispontaneous occupancy of the $8a$ site. It is worth noting that in most of the cation-antisite configurations studied here, an O_{48f}^{2-} moves into a $V_{O_{8a}}$ site after full relaxation. The projected density of states (PDOS) obtained from the HF calculations for $0X$ and $2X + (V_{O_{48f}}^{\cdot\cdot} + O_{8a}^{2-})$ configurations are shown in Figs. 4 and 5, respectively. A detailed analysis shows that the increase in cation disorder ($2X$) with the simulteneous occupancy of the oxygen $8a$ site leads to a considerable decrease of the energy gap from 16.5 eV to 11.3 eV, which is close to the value of 13.1 eV calculated for ZrO_2 by a similar *ab initio* method.[51] The occupancy of the $8a$ site is principally responsible for the lowering of the
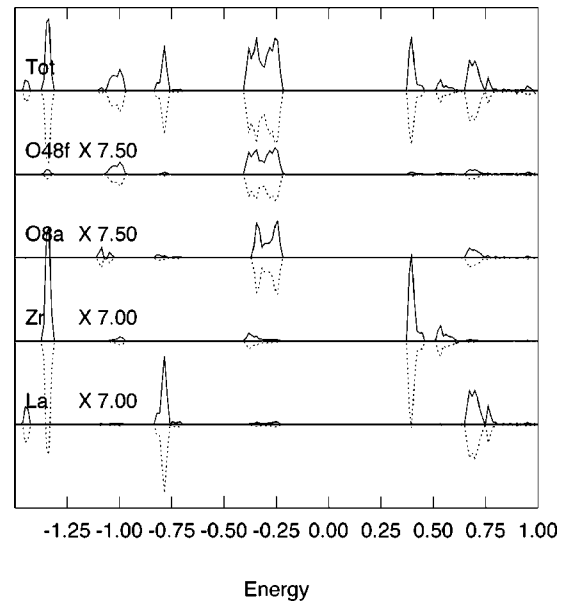

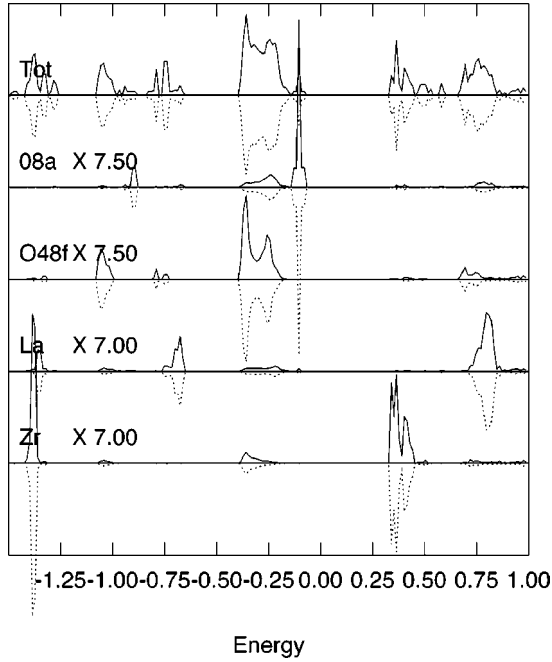FIG. 4. Projected densities of states (PDOS) for ordered $La_2Zr_2O_7$.

FIG. 5. Projected densities of states (PDOS) for $La_2Zr_2O_7$ with $2X + (V_{O_{48f}}^{..} + O_{8a}^{2-})$.

energy gap. This can be clearly seen in Fig. 6, which shows the change in the energy gap given by ΔE_g, determined from the HF single-point-energy calculation at intermediate coordinates as the oxygen in the $48f$ position displaces to the vacancy at the $8a$ site for the ordered $(0X)$ state. It is interesting to note that the Mulliken charge decreases slightly along this displacement, demonstrating further the validity of the AIP used here when considering the occupation of the $8a$ site. As the titanium concentration increases, the Frenkel-pair formation energy of $O_{8a}^{2-} + V_{O_{48f}}^{..}$ increases, thus introducing an opposite effect than that caused by increasing the disorder.

The addition of the O_{8a}^{2-}-occupancy energy to the vacancy formation energies of $V_{O_{48f}}^{..}$ and $V_{O_{8b}}^{..}$ gives an estimation of the extended Frenkel-pair energies as given in Table VII. The
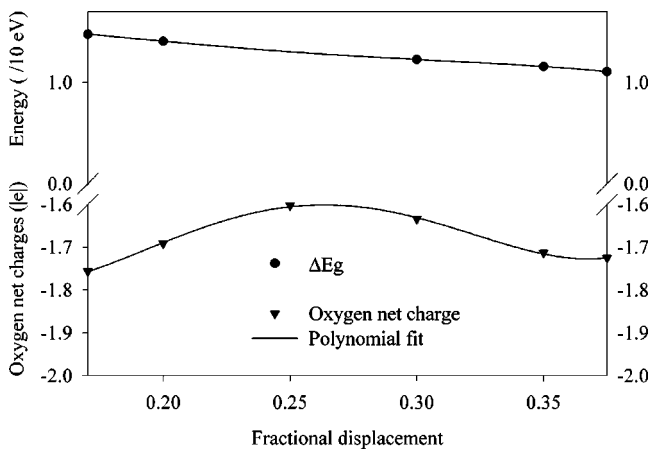

FIG. 6. Plots of band gap ΔE_g, and O_{48f} Mulliken charge variation when displaced toward the $V_{O_{8a}}$ site in the primitive cell of $La_2Zr_2O_7$.

TABLE VIII. Defect-formation energies for cations (eV/defect) in different antisite disorders, with and without titanium. The cation interstitial site is the $32e$ site.

$La_2Zr_2O_7$ defects	Pure			Ti substituted for Zr	
	$2X$	$1X$	$0X$	$0X$-1Ti	$0X$-2Ti
V_{La}'''	48.41	46.37	46.30	46.50	46.25
F-V_{La}'''-La_i^{3+}	8.99	7.93	7.28	7.50	7.31
V_{Zr}''''	82.40	85.29	85.88	85.79	
V_{Ti}''''					92.21
F-V_{Zr}''''-Zr_i^{4+}	10.63	12.67	14.93	15.68	
F-V_{Ti}''''-Ti_i^{4+}				14.36	14.95

value of 3.06 eV obtained for the $O_{8a}^{2-} + V_{O_{48f}}^{..}$ Frenkel pair is in agreement with that of previous work.[23] This shows that increasing disorder considerably decreases the energies of the Frenkel pairs while, in contrast, increasing the substitution of zirconium with titanium increases the corresponding Frenkel-pair energies.

In Table VIII are given the calculated lanthanum, zirconium, and titanium isolated vacancies as well as the Frenkel-pair formation energies. In all the cases, in terms of energy, the V_{La}''' are less expensive to create by about 50% compared to V_{Zr}'''', the latter ones being roughly 10% less expensive than V_{Ti}''''. The disorder increases the formation energy of V_{La}''' and decreases that of V_{Zr}''''. This influence appears clearly on the corresponding Frenkel-pair formation energies, tending to a homogenous value of about 10 eV. It is worth comparing this value to those obtained for the zirconium Frenkel pairs in tetragonal and cubic zirconia, which are 8.8 eV and 10.1 eV, respectively.[57] For comparison, the titanium Frenkel-pair formation energy in Ti-doped $La_2Zr_2O_7$ is close to 15 eV, hence 50% higher than that found for zirconia.

In summary, no significant points can be extracted regarding the influence of titanium on the cation vacancies and the Frenkel formation energies in the titanium-doped $La_2Zr_{2(1-y)}Ti_{2y}O_7$, at least for simulated concentrations lower than $y \lesssim 0.5$. However, the close and extended O_{8a}^{2-}-$V_{O_{48f}}^{..}$ Frenkel pairs cost more energy to create as the Ti concentration is increased. The Ti-vacancy and Frenkel-pair energies are also clearly higher than those of Zr. Whereas, in absence of Ti, the disorder effect appears to be dominant enough for tending to homogenize the cation-Frenkel formation energies and by strongly favoring the occupation of the $8a$ site by both O_{48f} and O_{8b}.

V. ACTIVATION ENERGIES FOR LATTICE MIGRATION

The behavior of $La_2Zr_2O_7$ under irradiation requires a detailed understanding of the defect-migration mechanisms that lead to structural transitions. The formation energies of cation-antisite and Frenkel-pair configurations are complemented by calculations of the activation energies for the migration of cations and anions to corresponding vacancies, which includes antisites of the cation sublattices and antisites of the distinct anion sublattices. The activation barriers are

TABLE IX. Activation energies for oxygen-lattice migration (in eV) to adjacent vacancies. The notation (1), (2), and (3) represents the migration paths of the oxygen ions in the $48f$ sites towards the $8a$ vacancy, see Fig. 1.

La$_2$Zr$_2$O$_7$ defects	Pure			Ti substituted for Zr	
	$2X$	$1X$	$0X$	$0X$-1Ti	$0X$-2Ti
O$^{2-}_{48f} \rightarrow V^{\cdot\cdot}_{O_{48f}}$ (1)	1.48	1.14	1.13	1.23	0.30
O$^{2-}_{48f} \rightarrow V^{\cdot\cdot}_{O_{48f}}$ (2)	0.85	0.45	1.01	0.49	
O$^{2-}_{48f} \rightarrow V^{\cdot\cdot}_{O_{48f}}$ (3)	0.86	2.36	0.92	1.68	0.96
O$^{2-}_{48f} \rightarrow V^{\cdot\cdot}_{O_{8b}}$	1.04	0.34	0.37	0.29	0.23
O$^{2-}_{8b} \rightarrow V^{\cdot\cdot}_{O_{48f}}$	2.70	0.49	0.42	0.29	0.14
O$^{2-}_{8a} \rightarrow V^{\cdot\cdot}_{O_{48f}}$	1.12	1.51	1.98	1.15	0.33
O$^{2-}_{48f} \rightarrow V_{O_{8a}}$	1.11	0.93	0.46	0.44	0.31

determined as in transition-state theory by searching for saddle points, which is done by using the rational-function-optimization method (RFO) or eigen-vector-following[43] routine as implemented in the GULP code. In the latter approach, the ion is displaced towards an adjacent vacancy calculating at each coordinate the eigenvalues of the Hessian (the energy second-derivatives matrix). The nth-order transition state corresponds to a saddle point with n imaginary eigenvalues of the Hessian. In this way, the activation energies were calculated for the first-order homoatomic and heteroatomic cation-lattice migration, as well as for those characterizing the anion displacements. The results are shown in Tables IX and X.

The calculated activation energies (Table IX) characterizing the migrations $O^{2-}_{48f} \rightarrow V^{\cdot\cdot}_{O_{48f}}$ in the ordered ($0X$) La$_2$Zr$_2$O$_7$ vary from 0.92 eV to 1.13 eV, in good agreement with those published previously that range from 1.05 eV to 1.10 eV.[58] Two different experimental measurements of the mean activation energy for the oxygen migration in this pyrochlore have been published, 0.49 eV (Ref. 59) and 0.74 eV.[60] Those values are in the range determined for Gd$_2$Zr$_2$O$_7$ where Catchen and Rearick[54] measured an activation energy of 0.25 eV for local hopping of the oxygen anion while Tsoga et al.[61] determined a value of 0.8–0.9 eV for long-range migration. Taking into account the fact that the calculated activation energies for the transitions $O^{2-}_{48f} \rightarrow V^{\cdot\cdot}_{O_{8b}}$ and $O^{2-}_{48f} \rightarrow V_{O_{8a}}$ in La$_2$Zr$_2$O$_7$ are 0.37 and 0.46 eV, respectively, while those of $O^{2-}_{48f} \rightarrow V^{\cdot\cdot}_{O_{48f}}$ are in the range 0.92–1.13 eV,

TABLE X. Cation-activation energies for lattice migration (in eV) to adjacent cation vacancies. The two first lines and the two last ones concern homoatomic and heteroatomic migrations, respectively. Symbols are defined in Table III.

La$_2$Zr$_2$O$_7$ defects	Pure			Ti substituted for Zr	
	$2X$	$1X$	$0X$	$0X$-1Ti	$0X$-2Ti
La$^{3+} \rightarrow V'''_{La}$	2.78	2.36	2.62	2.78	3.42
Zr$^{4+} \rightarrow V''''_{Zr}$	6.11	3.32	3.87	2.65	1.84
La$^{3+} \rightarrow V''''_{Zr}$	5.79	3.48	2.71	4.05	5.92
Zr$^{4+} \rightarrow V'''_{La}$	9.26	7.94	6.96	8.60	9.98

the values calculated in this work are consistent with experiments. Concerning the anions, the disorder renders the activation energies roughly equal to 1 eV, which is generally the case in the fluorite structures and more specifically for zirconia in which the activation energies for the oxygen migration are estimated to be in the range 0.8–0.9 eV.[62–64]

The activation energies for homoatomic and heteroatomic cation migration (Table X) increase steadily with increasing disorder. It is interesting to note that the mean value of all the possible transitions tends to about 6 eV, which is close to that estimated for zirconium in stabilized zirconia ZrO$_2$.[65,66]

The presence of titanium ions have the net influence of considerably lowering the anion-activation energies, in agreement with previous observations.[67] In contrast, the inclusion of titanium ions increases the activation energies for homoatomic La and heteroatomic La and Zr migration, whereas, there is a decrease in activation energy for homoatomic Zr migration with increasing Ti substitution.

VI. CONCLUSIONS

In this paper, the coupling of interatomic-potential models and *ab initio* calculations was used to obtain atomic-level details of the formation and activation energies of principal defects in La$_2$Zr$_{2(1-y)}$Ti$_{2y}$O$_7$ pyrochlore at low titanium concentrations ($0 \leqslant y \leqslant 0.5$). The purpose was to extract the relevant trends affecting the transition of the ordered pyrochlore to a cation-disordered structure, which could be associated with irradiation damage and the influence of titanium substitution on this.

In the ordered pyrochlore the cation-antisite formation energies of 2 and 3.4 eV for $1X$ and $2X$, respectively, are rather low. Under these conditions, it can be deduced that the accumulation of antisite configurations yields an energetically stable phase that could be similar to an irradiation-induced state. Such a state could become even more stable with increasing disorder since in a disordered structure the absolute values of cation-antisite formation energies are lowered to about 1.5 and 3 eV for $1X$ and $2X$ respectively. At the same time, the propensity of the pyrochlore structure to fill the vacant oxygen $8a$ site becomes even stronger and the disorder favors the random occupancy of these sites. The tendency towards this behavior may have a direct physical consequence along the propagation path of an irradiating particle in a zirconate pyrochlore structure. A continuous mechanism of cation inversion accompanied by oxygen Frenkel-pair formation at the 8a site may easily dissipate a considerable part of the kinetic energy of the ballistic process by forming a disordered structure. As a result of structural modification, physical properties associated with the ordered pyrochlore will tend to homogeneous values that are comparable to those of the zirconia fluorite structure. In fact, in the disordered state the pyrochlore $48f$ and $8b$ oxygen sites vanish where the oxygen charges tend to a unique value. Simultaneously, the activation energy for the anion migration, which characterizes the ionic conductivity, tends to 1 eV, which is comparable to that of 0.8–0.9 eV in zirconia. The mean cation-migration energy from a lattice site to a vacancy gets close to 6 eV and the Frenkel-pair formation energy tends to

10 eV, also equivalent to those estimated in zirconia. Finally the energy gap decreases from 16.5 eV to 11.3 eV approaching the value of 13.1 eV calculated previously for cubic zirconia.

An essential difference has been found for the cation-antisite formation energies between the ordered and the disordered state. The ordered pyrochlore structure exhibits an important resistance towards any internal transformation that weakens with the accumulation of cation antisites. This indicates that the introduction of partial disorder, by whatever means, facilitates the cation-antisite formation. A more detailed study that considers both the statistical distributions of cation-antisite configurations with random occupancies of the $8a$ site and the activation energies for the formation of cation antisites could further confirm this point.

The titanium influence has been investigated at low concentrations. However, some interesting trends arise from these calculations. There is a significant difference between the Zr-La antisite formation energies and the Ti-La ones, the latter being considerably higher in both the ordered pyrochlore and the disordered structure. Furthermore, titanium is unfavorable to the occupancy of the oxygen $8a$ vacant site by increasing the corresponding close and extended Frenkel formation energies. The coupling of these effects contribute in preventing the titanium-substituted pyrochlore structure from transforming towards the disordered fluorite.

---

*Electronic address: meis@carnac.cea.fr

†Electronic address: rene.corrales@pnl.gov

[1] See, for example, *Radioactive Waste Forms for the Future*, edited by W. Lutze and R.C. Ewing, (North-Holland, Amsterdam, 1988).

[2] I. Hayakawa and H. Kamizono, J. Nucl. Mater. **202**, 163 (1993).

[3] P. Zhao, W.L. Bourcier, B.K. Esser, and H.F. Shaw, in *Plutonium Futures-The Science*, edited by K.K.S. Pillay and K.C. Kim, AIP Conf. Proc. No. 532 (AIP, Melville, NY, 2000), p. 157.

[4] G.R. Lumpkin, J. Nucl. Mater. **289**, 136 (2001).

[5] R.A.V. Konynenburg, Lawrence Livermore National Laboratory, Technical Report No. UCRL-ID-128580, 1997.

[6] D.M. Strachan, R.D. Steele, W.C. Buchmiller, J.D. Vienna, R.L. Sell, and R.J. Elovich, Pacific Northwest National Laboratory, Technical Report No. PNNL-13251, 2000.

[7] W.J. Weber *et al.*, J. Mater. Res. **13**, 1434 (1998).

[8] W.J. Weber and R.C. Ewing, Science **289**, 2051 (2000).

[9] G.R. Lumpkin, K.L. Smith, and M.G. Blackford, J. Nucl. Mater. **289**, 177 (2001).

[10] S.X. Wang, B.D. Begg, L.M. Wang, R.C. Ewing, W.J. Weber, and K.V.G. Kutty, J. Mater. Res. **14**, 4470 (1999).

[11] S.X. Wang, L.M. Wang, R.C. Ewing, G.S. Was, and G.R. Lumpkin, Nucl. Instrum. Methods Phys. Res. B **148**, 704 (1999).

[12] B.D. Begg, N.J. Hess, W.J. Weber, R. Devanathan, J.P. Icenhower, S. Thevuthasan, and B.P. McGrail, J. Nucl. Mater. **288**, 208 (2001).

[13] K.E. Sickafus, L. Minervini, R.W. Grimes, J.A. Valdez, M. Ishimaru, F. Li, K.J. McClellan, and T. Hartmann, Science **289**, 748 (2000).

[14] B.D. Begg, N.J. Hess, D.E. McCready, S. Thevuthasan, and W.J. Weber, J. Nucl. Mater. **289**, 188 (2001).

[15] J. Flahent, *Les éléments des Terres Rares*, Collection de Monographies de Chimie (Masson et Cie, Paris 16ème, 1969).

[16] T.G. Chirayil, M. Paranthaman, D.B. Beach, D.F. Lee, A. Goyal, R.K. Williams, X. Cui, D.M. Kroeger, R. Feenstra, and D.T. Verebelyi, Physica C **336**, 63 (2000).

[17] R.E. Williford, W.J. Weber, R. Devanathan, and J.D. Gale, J. Electroceram. **3**, 409 (1999).

[18] D. Chen and R. Xu, Mater. Res. Bull. **33**, 409 (1998).

[19] A.K. Battacharya, A. Hartridge, K.K. Mallick, and J.L. Woodhead, J. Mater. Sci. **29**, 6076 (1994).

[20] Y. Tabira, R.L. Withers, J. Thompson, and S. Schmid, J. Solid State Chem. **142**, 393 (1999).

[21] Y. Tabira and R. Withers, Philos. Mag. A **79**, 1335 (1999).

[22] N.K. Kulkarni, S. Sampath, and V. Venugopal, J. Nucl. Mater. **281**, 248 (2000).

[23] P.J. Wilde and C.R.A. Catlow, Solid State Ionics **112**, 173 (1998).

[24] R.E. Williford, W.J. Weber, R. Devanathan, and J.D. Gale, J. Am. Ceram. Soc. **82**, 3266 (1999).

[25] T. Omata, K. Okuda, S. Tsugimoto, and S. Otsuka-Matsuo-Yao, Solid State Ionics **104**, 249 (1997).

[26] H. Yokoi, Y. Arita, T. Matsui, H. Ohno, and K. Kobyashi, J. Nucl. Mater. **238**, 163 (1996).

[27] M. Bolech, E.H.P. Cordfunke, A.C.G. van Genderen, R.R. van der Lann, F.J.J.G. Janssen, and J.C. van Miltenburg, J. Phys. Chem. Solids **58**, 433 (1997).

[28] J.A. Labrincha, J.R. Frade, and F.M.B. Marques, J. Mater. Sci. **28**, 3809 (1993).

[29] R. Vassen, X. Cao, F. Tietz, D. Basu, and D. Stöver, J. Am. Ceram. Soc. **83**, 2023 (2000).

[30] V.R. Saunders, R. Dovesi, C. Roetti, M. Causà, N.M. Harrison, R. Orlando, and C.M. Zicovich-Wilson, CRYSTAL98 user's manual (University of Torino, Torino, Italy, 1998).

[31] J.D. Gale, J. Chem. Soc., Faraday Trans. **93**, 629 (1997).

[32] J.H. Harding, Mol. Simul. **4**, 255 (1990).

[33] M.A. Subramanian, G. Aravamudan, and C.V.S. Rao, Prog. Solid State Chem. **15**, 55 (1983).

[34] Computer code, CASTEP (Accelrys, San Diego, CA, 1998).

[35] R. Dovesi, C. Roetti, C. Freyra-Fava, E. Aprà, V.R. Saunders, and N.M. Harrison, Philos. Trans. R. Soc. London, Ser. A **341**, 203 (1992).

[36] C. Pisani, R. Dovesi, and C. Roetti, *Hartree-Fock Ab Initio Treatment of Crystalline Systems*, Lectures notes in Chemistry (Springer-Verlag, Heidelberg, 1988), Vol. 48.

[37] See http://www.ch.unito.it/ifm/teorica/Basis_sets/mendel.html

[38] J.P. Perdew, *Electronic Structure of Solids 91* (Springer-Verlag, Berlin, 1991).

[39] J.P. Perdew, J.A. Chevary, S.H. Vosko, K.A. Jackson, M.R. Pederson, D.J. Singh, and C. Fiolhais, Phys. Rev. B **46**, 6671 (1992).

[40] B.G. Dick and A.W. Overhauser, Phys. Rev. **112**, 90 (1958).

[41] W. Kohn and L.J. Sham, Phys. Rev. A **140**, 1133 (1965).

[42] N. Mott and M. Littleton, Trans. Faraday Soc. **34**, 485 (1938).

[43] A. Banarjee, N. Adams, J. Simons, and R. Shepard, J. Phys. Chem. **89**, 52 (1985).

[44] H.W. Schmalle, T. Williams, A. Reller, A. Linden, and J.G. Bednorz, Acta Crystallogr., Sect. B: Struct. Sci. **B49**, 235 (1993).

[45] M. Born and H. Kun, *Dynamical Theory of Crystal Lattices*, The International Series of Monographs on Physics (Oxford Science, Oxford, 1985).

[46] J.P. Poirier, *Introduction to the Physics of the Earth's Interior*, Cambridge Topics in Minerals Physics and Chemistry Vol. 3 (Cambridge University Press, Cambridge, 1991).

[47] M. Catti, R. Dovesi, A. Pavese, and V.R. Saunders, J. Phys.: Condens. Matter **3**, 4151 (1991).

[48] A. Lichanot, Solid State Commun. **116**, 543 (2000).

[49] R. Orlando, C. Pisani, C. Roetti, and E. Stefanovich, Phys. Rev. B **45**, 592 (1992).

[50] J. Muscat, N.M. Harrison, and G. Thornton, Phys. Rev. B **59**, 2320 (1999).

[51] S. Gennard, F. Corà, and C.R.A. Catlow, J. Phys. Chem. **103**, 10158 (1999).

[52] C.R.A. Catlow, Proc. R. Soc. London, Ser. A **333**, 533 (1977).

[53] L. Minervini, R.W. Grimes, and K.E. Sickafus, J. Am. Ceram. Soc. **83**, 1873 (2000).

[54] G.L. Catchen and T.M. Rearick, Phys. Rev. B **52**, 9890 (1995).

[55] J.B. Thomson, A.R. Armstrong, and P.G. Bruce, J. Am. Chem. Soc. **118**, 11129 (1996).

[56] H. Takamura and H.L. Tuller, Solid State Ionics **134**, 67 (2000).

[57] D. Bingham, P.W. Tasker, and A.N. Cormack, Philos. Mag. A **60**, 1 (1989).

[58] M. Pirzada, R.W. Grimes, L. Minervini, J.F. Maguire, and K.E. Sickafus, Solid State Ionics **140**, 201 (2001).

[59] F.W. Poulsen and N. van der Puil, Solid State Ionics **53-56**, 777 (1992).

[60] G. Chiodelli and M. Scagliotti, Solid State Ionics **73**, 265 (1994).

[61] A. Tsoga, A. Naoumidis, and D. Stöver, Solid State Ionics **135**, 403 (2000).

[62] N. Bonanos and E.P. Butler, J. Mater. Sci. Lett. **4**, 561 (1985).

[63] W.C. Mackrodt and P.M. Woodrow, J. Am. Chem. Soc. **69**, 277 (1986).

[64] D. Bingham, C.A. Leach, and B.C.H. Steele, Mater. Sci. Technol. **3**, 401 (1987).

[65] K. Kowalski, A. Bernasik, and A. Sadowski, J. Eur. Ceram. Soc. **20**, 951 (2000).

[66] M. Matsuda, J. Nowotny, Z. Zhang, and C.C. Sorrell, Solid State Ionics **111**, 301 (1998).

[67] J.T.S. Irvine, A.J. Feighery, D.P. Fagg, and S. García-Martin, Solid State Ionics **136-137**, 879 (2000).